IEEE Access
Multidisciplinary | Rapid Review | Open Access Journal

Received 26 September 2024, accepted 7 November 2024, date of publication 11 November 2024,
date of current version 20 November 2024.

Digital Object Identifier 10.1109/ACCESS.2024.3495560

RESEARCH ARTICLE

Transformer-Based Deep Learning Strategies for Lithium-Ion Batteries SOX Estimation Using Regular and Inverted Embedding

JOHN GUIRGUIS[1], AHMED ABDULMAKSOUD[1], MOHANAD ISMAIL[1], PHILLIP J. KOLLMEYER[2], (Member, IEEE), AND RYAN AHMED[1]

[1]Department of Mechanical Engineering, McMaster University, Hamilton, ON L8S 4L8, Canada
[2]Department of Electrical and Computer Engineering, McMaster University, Hamilton, ON L8S 4L8, Canada

Corresponding author: John Guirguis (guirgj5@mcmaster.ca)

ABSTRACT The accurate estimation of Li-ion battery (LIB) states such as State of Charge (SOC), State of Health (SOH), and State of Power (SOP) plays a pivotal role in the efficient operation of Electric Vehicles (EVs). These parameters can impact the battery's health, driving range, and overall vehicle performance. Transformer-based artificial neural networks have shown impressive results in natural language processing (NLP) and estimation problems of many other domains. This paper presents an intensive study on the capabilities of various Transformer-based models in estimating the SOC and SOH of LIBs, the SOP is obtained based on the estimated SOC. This paper provides the following key original contributions: 1) the application of the Informer and Reformer variants of the Transformer model for the first time for SOH estimation of LIBs in EVs, 2) studying the effect of inverted embedding of iTransformers, a modified architecture of the transformers, on SOC and SOH estimation, inversion is performed on the Informer and Reformer as well; 3) applying a simple feature extraction method using partial discharge cycles for SOH estimation with Transformer-based models; 4) a new robust method is proposed for SOC estimation based on a 2-Encoder-Transformer with a one-dimensional convolutional neural network (1D-CNN) architecture; 5) the various architectures are trained, validated and tested on two real-world datasets comprising various driving scenarios and battery conditions. Comparative analysis with various deep learning architectures show impressive accuracy for estimating the SOC and SOH, leading to better SOP calculation.

INDEX TERMS Convolutional neural networks, deep learning, electric vehicles, iTransformers, li-ion batteries, state estimation, state of charge, state of health, state of power, transformers.

I. INTRODUCTION

The automotive industry faces several challenges that have not been witnessed in decades. In an era that emphasizes a strong need for energy optimization, independence of the human role, performance improvements, and elimination of warm gas emissions, most vehicle manufacturers are expanding their electrification efforts to replace conventional internal combustion engine (ICE) vehicles with more clean and efficient alternatives [1]. With a global warming increase of around 1°C over pre-industrial temperatures attributed to human activities [2], the world is looking for paths to address this issue. One such path is electrification, which is expected to reduce CO2 emissions from currently expected scenarios by up to 15% by 2030 [3].

The automotive industry is shifting towards AI-powered [4], [5], cloud-integrated Battery Electric Vehicles (BEVs) at an unprecedented pace. These BEVs reduce air pollution and offer a sustainable, low-maintenance alternative compared to traditional ICE-powered vehicles. In response, nations like Canada, the European Union, and Japan are mandating all newly sold light-duty vehicles and passenger trucks to be BEVs by 2035 to meet net-zero emissions by 2050 goals [6], [7]. Top automotive companies like GM and Ford are embracing this electric transition by committing to an all-electric future and phasing out ICE-powered vehicles. BEVs are strategically crucial in strengthening countries' energy security by leveraging locally produced electricity, therefore

The associate editor coordinating the review of this manuscript and approving it for publication was Bing Li.

eliminating the need for imported energy, which became of utmost importance for governments after the recent geopolitical tension and the war in Ukraine. To accomplish these ambitious strategic objectives, Original Equipment Manufacturers (OEMs) must focus on achieving cost parity with comparable ICE-powered vehicles, expediting battery charging, extending driving ranges, centralizing software architecture, and incorporating cloud connectivity. Many challenges face the widespread adoption of BEVs: (1) the high cost of Li-Ion battery (LIB) packs due to over-engineering and battery management system (BMS) limitations, (2) battery aging and degradation, (3) long charging times, (4) customer range anxiety, (5) BEVs' resale cost, and aftermarket value, dramatically reduced if the battery pack is aged, (6) safety considerations due to fire and thermal runaway.

Many of the listed challenges that face BEVs arise from the fact that the state of charge (SOC) of LIBs, the state of health (SOH), together with the state of power (SOP), cannot be directly measured by any sensing means. That is why comprehensive research studies are always conducted using various techniques to enhance the estimation of these states in a competitive, accurate fashion. The SOC is the amount of charge remaining in the battery as a percentage of its current total capacity. The simplest way to calculate the SOC is the Coulomb Counting approach in which the integration of the current intensity passing through the cell over time calculates the amount of charge entering or leaving the cell [8], [9]. Although easy to implement in the BMS onboard vehicles, Coulomb Counting possesses many weaknesses [10]; it requires knowledge of the initial SOC value to add up to it, as it is a relative calculation, not an absolute one; it does not consider the aging of the battery; and being an open-loop calculation method, it may have a significant cumulative error. The SOH is a quantitative index of how far the battery is from healthy/fresh conditions and is modeled in many studies as a decrease of the original capacity of the cell (SOHc) and/or an increase of its internal resistance (SOHr) [11]. Experimental methods that involve direct measurements of parameters such as the battery's current and using it along with other analysis methods, like incremental capacity analysis [12], [13], can be used to determine the age and health of LIBs [14]. However, these methods are impractical, as they require some conditions that are difficult to fulfill during the real operation of an EV battery, such as low currents, which cannot be guaranteed [14]. Regarding the power capabilities of a battery, the SOP is an index of the maximum power at which an electric battery can charge or discharge [15]. The SOP is usually obtained using a characteristic map expressing its dependency on SOC, SOH, and temperature. No datasets are related to SOP to the authors' best knowledge. For that reason, SOP is usually calculated using other estimated states of the battery, such as the SOC and SOH.

The difficulties that face the direct finding of these three states of a battery led to the need for other indirect estimation techniques. These methods are classified as either model-based or data-driven. In model-based estimation, a mathematical model of the battery, such as the equivalent circuit model (ECM) or the electrochemical model, is developed. However, developing a model that accurately describes the dynamics of the battery across the entire range of SOC, SOH, and temperature is not straightforward due to the uncertainties and nonlinear nature of the cell. That is why closed loop filters are often used alongside these models; to correct their obtained states based on other measurable states as the terminal voltage (V_T) [16], [17], [18], [19], [20], [21], [22]. Electrochemical models are computationally expensive compared to other methods, which leads to challenges in online SOH estimation [23]. ECMs are faster and more efficient but do not offer satisfactory accuracy for SOH estimation [24].

The recent advancements in Artificial Intelligence (AI) highlight the effectiveness of data-driven approaches, which offer a compelling solution to the SOX estimation challenges faced by model-based methods [25]. AI is a revolutionary technology that can work as a critical enabler in increasing the widespread adoption and acceptance of BEVs and solving the challenges above. According to the 2023 AI Index Report released by the Stanford Institute for Human-Centered Artificial Intelligence (HAI), AI continued to demonstrate state-of-the-art performance and has accelerated scientific advancement at an unprecedented pace, notably contributing to breakthroughs in hydrogen fusion and the generation of new antibodies [26]. The adoption rate of AI within companies increased by twofold in 2022 compared to 2017, while private investments in AI were 18 times greater than it was in 2013 [26]. Without the need for any deep knowledge of the battery's chemical and physical nature, an AI model can be trained using large datasets to mimic the behavior of the battery.

AI sequence-based models have shown superior results in the modeling of time-series problems [27], [28], [29]. This encourages the use of models such as Recurrent Neural Networks (RNNs) and Long Short-Term Memory (LSTMs) for the modeling of EV batteries [30]. LSTMs have been used in SOC estimation as in [31] to implicitly capture the highly non-linear internal dynamics of the battery. Bi-directional RNNs (Bi-RNNs) [32] have also been employed in estimating the battery states, capturing temporal correlations, and ensuring better SOC estimation across different drive-cycles with better accuracy. However, LSTMs and RNNs still struggle with long-sequence problems due to their sequential nature and memory constraints, dramatically increasing complexity.

Since the rise of the attention-based models that are used in the transformer architecture [33], and its success in many applications such as Natural Language Processing (NLP), speech recognition, and computer vision, there has been a motivation to apply it for the estimation of the battery states; due to the sequential nature of the problem. Sitapure et al. explored multiple sequence-based architectures, including LSTMs and Time-Series-Transformers (TSTs), for battery states prediction [34]. They conducted a thorough study

involving a dataset that contains 72 different driving trips performed using a 660Ah BMW I3 Battery. They compared LSTM, encoder-TST (enc-TST), Vanilla-TST (v-TST), TST-LSTM, and encoder TST decoder LSTM (enc-TST-dec-LSTM). Their results showed that the v-TST performed better than an LSTM, which also performed better than the other hybrid models. Their analysis concluded that integrating TST and LSTM into a hybrid model led to an additional layer of complexity and an imbalance in the model structure. This potentially disrupted the flow of information and compromised the model's ability to generalize. This integration also led to the hybrid models losing the attention mechanism and overfitting due to having more parameters. Shen et al. designed a transformer model for SOC prediction with invariance adaptive observer that effectively narrowed the battery parameters prediction error and showed improved performance over models based on the LSTM [35]; moreover, an interesting approach taken in this paper is the separation of each of the inputs (current and voltage) into different encoders and concatenating the result in the end. This allows the model to learn the features of each input over the whole sequence rather than a single data point. Their method, however, needs to receive the entire length of the input sequence length after predicting one value. This means that the model can produce a prediction after time steps equal to the input sequence length, rather than each time step. Yi et al. [36] then improved on the accuracy of the aforementioned models by addressing the over-stationarization problem. A shortcoming of this model is not taking the aging of the battery into account when predicting the SOC.

Transformer-based architectures, however, are not without drawbacks. A significant problem that faces transformers is their large computational and memory requirements, especially with longer input sequences. Since each data point needs to be processed with respect to all other data points, the complexity is found to be $O(L^2)$. [37] addresses this issue by proposing a modified transformer architecture called an Informer. It introduces a ProbSparse self-attention mechanism, lowering the complexity to $O(Llog(L))$. Zhou et al. [38] achieve a similar improvement in complexity by using locality-sensitive hashing for attention, naming this new architecture the Reformer.

This paper examines the performance of various Transformer-based models, utilizing regular and inverted embedding [39], to predict the SOC and SOH of LIBs. The SOH estimation is based on a simple feature extraction from partial discharge cycles, this method is proved to be efficient with Transformer-based models. The study proposes a robust architecture for SOC estimation based on a 2-Encoder Transformer followed by a one-dimensional convolutional neural network (1D-CNN). The most accurate SOC estimate is then used to determine the SOP. The proposed methods are validated on real-world datasets through a comparative analysis with multiple DL models from [40] and [41]

The remainder of this paper is organized as follows: Section II covers the SOH estimation and presents the models, dataset, and experimental results comparing the tested models; Section III emphasizes the same details for SOC estimation; while Section IV explains the calculations of obtaining the SOP; and finally, Section V concludes the manuscript and lays future work.

II. STATE OF HEALTH ESTIMATION

A. MODEL ARCHITECTURES

This section lays out the details of the architectures that are used and compared to estimate the SOH. The foundation of the Transformer model [33], which serves as the building block for the iTransformer-based architecture, is presented. Other variations of the Transformer are also emphasized (Informer [37] and Reformer [38]). These variants were developed to enhance the Transformer's time series forecasting capabilities. The inverted-embedding method is then introduced and integrated with the Transformer architecture (iTransformer [39]). This section compares the Transformer, Reformer, Informer, and their inverted versions in estimating the SOH of LIBs.

1) TRANSFORMER, INFORMER AND REFORMER MODELS

Transformers were introduced by Vaswani et al. [33] to tackle the limitations of previous architectures, such as RNNs, LSTMs, and Gated Recurrent Units (GRUs) in long-sequence forecasting. This is done by employing *Attention*. This mechanism allows the model to select parts of the sequence with the most significance to the output. It also allows greater data parallelization during training and inference by escaping recurrence.

As shown in Fig. 1, the Transformer model is composed of three main components: input embedding, the encoder, and the decoder. For the input embedding, the tokens are embedded along the variate dimension to allow the mapping of the input data to a higher dimensional space d_{embed}, which allows the model to understand the data more effectively. The resulting embedding is then added to positional encoding, which enables the model to make use of the order of the sequence in the absence of recurrence. The shape of the resulting output of data embedding and positional encoding is $(Batch\_size \times d_{embed} \times sequence\_length)$.

Multi-head Attention, which is the building block of the Transformer model, is then applied to the embedded input. The attention function can be described as mapping a query and a set of key-value pairs to an output. Thus, each attention head uses three neural networks to map a part of the input embedding into *Query* (Q), *Key* (K), and *Value* (V). *Scaled Dot-Product* is then computed by applying dot-product between Q and K, dividing by the dimension of k (d_k), and applying a softmax function to get a weight on the output values. Following that, the weighted matrix is multiplied by V to obtain the output. The output of the attention head altogether can be computed as in Eq. 1:

$$Attention(Q, K, V) = softmax(\frac{QK^T}{\sqrt{d_k}})V \quad (1)$$

N attention heads are applied on d_{embed}/N partitions of the data embedding instead of a single attention function to allow the model to focus on different parts of the input sequence simultaneously, allowing each head to learn different relationships within the data, leading to a better representation.

A feed-forward neural network (FNN) with rectified linear unit (ReLU) activation is then applied to the concatenated attention maps from the attention heads. The output of the FNN is the output of a single encoder layer. In the original manuscript of Transformers [33] a stack of six identical encoder layers is employed on top of each other. The decoder has a similar architecture to that of the encoder. However, as observed in Fig. 1, two multi-head attentions are employed per decoder layer. The first is masked multi-head attention, which prevents the model from attending to future tokens during the generation process. The second attention head allows encoder-decoder attention. This enables the model to attend to relevant information from the encoder's output during decoding. Encoder-decoder attention empowers the model to leverage both information from the encoder and the decoder to generate contextually appropriate outputs. Six decoder layers are then stacked on top of each other before applying a fully connected layer to get the final output.

Since the introduction of the Transformer architecture, several studies have aimed to improve the complexity of self-attention, which has an $O(L^2d)$ time complexity where L is the sequence length and d is the embedding dimension. Zhou et al. in [37] presented the Informer that uses a *ProbSparse* self-attention which achieves $O(LlogL)$ time and space complexity. This is done by computing a *Query Sparsity Measurement* $M(q_i, K)$, which is calculated as in Eq. 2:

$$M(q_i, K) = ln \sum_{j=1}^{L_k} e^{\frac{q_i k_j^T}{\sqrt{d}}} - \frac{1}{L_K} \sum_{j=1}^{L_K} \frac{q_i k_j^T}{\sqrt{d}} \tag{2}$$

$M(q_i, K)$ is used to get $\hat{Q}$, which has the top-u queries from $M(q_i, K)$ representing the "most important" queries to use in the scaled dot-product. Doing that, the query lookup is reduced to $O(LogL_Q)$, where L_Q is the query dimension, and the query-key lookup in the ProbSparse attention is reduced to $O(L_K LogL_Q)$, where L_K is the key dimension. *Reformer* was also introduced by Kitaev et al. in [38] to address the time and space complexity of using attention. They proposed replacing the dot-product attention of [33] with locality-sensitive hashing attention; additionally, they further improve the efficiency of their architecture by using reversible residual layers, which allow one-time storing of activations instead of N-times storing. These enhancements have also reduced the complexity of computing attention to $O(LlogL)$, resulting in a faster and more memory-efficient model compared to that of the original Transformer model.

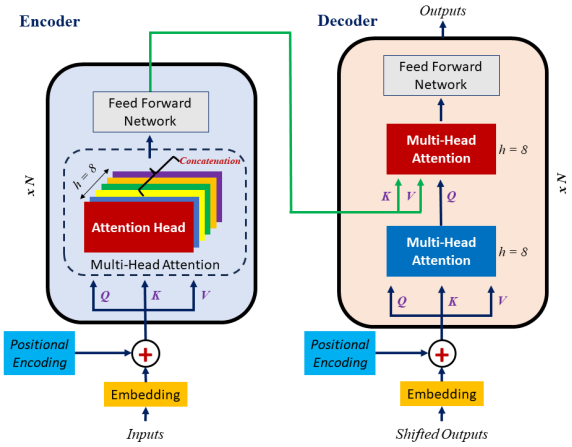

FIGURE 1. Basic transformer architecture from [33].

2) ITRANSFORMER ARCHITECTURE

Although the Transformer model presented a promising forecasting behavior with time-series problems, it still has problems with long look-back sequences that lead to computational complexity and accuracy degradation. Liu et al. in [39] addressed this issue by introducing an inverted architecture. Instead of formulating *temporal tokens* that consist of variates (features) at each time step, the iTransformer embeds *variate tokens*. This inversion which is illustrated in Fig. 2, is intended to eliminate this issue. The inverted embedding encourages *self-attention* to capture multi-variate correlations by learning meaningful representations of the attention maps. The model subsequently employs a fully connected network for each token to map the representations into the desired output.

For SOH experiments, the following model hyper-parameters have been followed: Two encoder layers and two attention heads per layer. The linear units use the Gaussian Error Linear Unit (GELU) activation function, this function is smooth over the entire input range and has non-monotonic behavior to capture complex patterns. The model dimension has been set to 512. During training, a batch size of 128 and a learning rate of 0.0005 are used, with an exponential decay scheduler set such that $lr \leftarrow 0.2 * lr^{\lfloor \frac{epoch}{2} \rfloor}$. The experiments were performed on an NVIDIA A100 80GB GPU. The architecture of the inverted models (iTransformer, iReformer, and iInformer), integrates the inverted embedding with the attention layer, forming the encoder-only architecture applied to the battery domain as shown in Fig. 3.

The loss function used to optimize the training of all models for **SOH and SOC estimation** is the mean square error (MSE) function, this is expressed in Eq. 3, where y is the ground true value, and y_{pred} is the predicted value for a total of N data points.

$$Loss = \frac{1}{N} \sum_{i=1}^{N} (y - y_{pred})^2 \tag{3}$$

B. DATASET

As mentioned in the introduction, the age and health of a battery are typically measured by the extent to which its

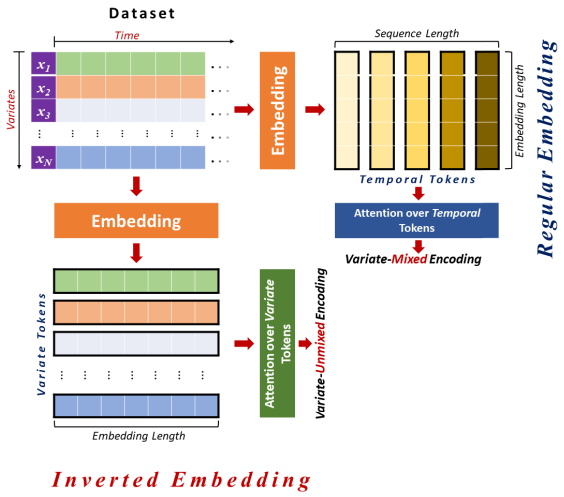

FIGURE 2. Variate Embedding vs temporal embedding.

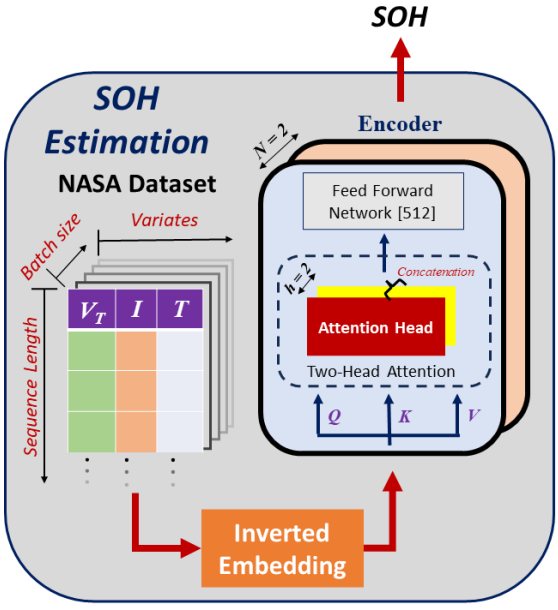

FIGURE 3. SOH estimation by iTransformers.

maximum capacity decreases and/or its internal resistance increases. These two factors determine the current range and power capabilities of the battery in comparison to when it was new. In this study, the SOH is determined based on the remaining capacity of the battery. The primary method for accurately estimating the SOH of a battery lies in analyzing its behavior while it charges or discharges. To test the aging of LIBs, aging tests [42], [43] usually subject a new battery to thousands of charging and discharging cycles that resemble real-life scenarios until it reaches specific end-of-life (EOL) criteria. Such tests have revealed that the battery's response in terms of its terminal voltage, temperature, and SOC profiles varies gradually as it ages despite subjecting it to the same input current profiles. This presents an opportunity to use a data-driven AI model that can discern features from vast training sets and predict the battery's age.

In this study, the SOH estimation is based on the data obtained from experiments conducted at NASA Ames Prognostics Center of Excellence (PCoE) [42]. The dataset provides actual values for the following measurements using a sampling rate of about 18 seconds:

1) The voltage measured at batteries' terminals. [Volts]
2) The output current of the batteries. [Amps]
3) Batteries temperature. [°C]
4) The voltage measured at the charger. [Volts]
5) The current measured at the charger. [Amps]
6) Time vector for the cycles. [Seconds]

These parameters are provided for the charging and discharging cycles for multiple *Li-Ion 18650* sized batteries at different temperatures. The batteries' voltage, current, and temperature [V, I, T] are utilized as input features to train the models under investigation, and the remaining capacity is the output.

In those aging experiments, the capacity test was repeated after discharging cycles to capture capacity fade, and the EOL is defined as 30% fade in rated capacity (*i.e.*, from 2 Ah to 1.4 Ah). This procedure results in a single SOH value for each complete discharge cycle which has hundreds of [V, I, T] points).

C. TEST CASES AND RESULTS

A series of comprehensive test cases was conducted to assess each model's ability to accurately track the SOH trends. For all of the test cases: 1) partial discharge cycles are used to train, validate, and test the models to ensure that the models are not just integrating the current intensity to infer the remaining capacity because the dataset uses a constant discharge current for all cycles; 2) the first 100 points ($\approx 1800 seconds$) only of each cycle are used to estimate the SOH at the end of the same cycle, where the length of the entire cycle ranges from 120 to 300 time steps (points); 3) B0005 only is used for training and the models are tested on B0006 and B0007.

1) TEST CASE 1

In the first case, the same SOH value is repeated for all 100 [V, I, T] points of each discharge cycle, as the problem involves many-to-one data. In training and testing, the models rely solely on the [V, I, T] as input features to infer the SOH. The results indicated that none of the models were able to track the SOH change in the two tested batteries accurately, and the predictions deviated significantly from the actual values.

2) TEST CASE 2

For this case, everything is similar to the previous one except that the estimated SOH for the previous cycle is fed as an input to the models together with the [V, I, T] profiles, the aim is to supply the model with a sequence of the previous targets to guide their next estimates. In training, the models acquire a previous sequence of the ground-truth SOH values, while during testing, they use their own previous predictions. The regular embedding models still struggle to track the SOH

and show significant deviation for the two batteries, while the inverted ones effortlessly generate a linear fit without capturing any trends.

3) TEST CASE 3

Instead of having multiple input points for each discharge cycle and repeating the output value for all of them, in this case, a simple feature extraction approach is followed to aggregate the first 100 time steps of each cycle into one feature point of voltage and temperature only, the current is removed as it has a constant value in all cycles and batteries. The SOH at that cycle is then used as the output. The models use their previous predictions as input. Aggregation is performed for each discharge cycle as follows, where V_{max} and V_{min} refer to the maximum and minimum voltage values in the first 100 steps:

- $V = V_{max} - V_{min}$
- T = *the variance of the temperature values*

Because the aggregation showed promising results, this test was repeated with three different sequence length values to further examine the impact of sequence length on estimation accuracy. For each sequence length, the model that gives the best fit together with the root mean square error (RMSE) values for all models is mentioned for the two tested batteries.

1) **Sequence Length = 1:** For a sequence length of 1, the inverted embedding models still produce a linear fit across the lifespan. However, the regular embedding demonstrates the ability to track output trends. The Reformer provided the best fit for B0006 (RMSE = 3.8%) and B0007. The minimum RMSE is 1.47% for the Reformer with B0007. Results in Fig. 4. The number of trainable parameters for the Reformer with SL of 1 is 2,640,897.
2) **Sequence Length = 48:** As the sequence length increases, the performance of the inverted models significantly improves, allowing them to better understand the input context. Among the models, the iInformer performs best with a sequence length of 48 for B0006, while the iReformer is the most suitable for B0007. The iReformer achieves a minimum RMSE of 0.98% for B0007. Fig. 5 shows the iReformer's behavior with B0007.
3) **Sequence Length = 96:** As the sequence length increases more, the performance is enhanced for both batteries. The Reformer gives the most accurate fit with inverted embedding for B0006 and regular embedding for B0007. The minimum RMSE is 0.74% for B0007 with the Reformer.

The findings from the test cases on estimating the SOH indicate that aggregating the aging data is the most effective method for preparing it for use with Transformer-based models. Inverted embedding requires variation in the target values to capture trends effectively. Models' performance on B0007 is always better (RMSE around 2% and as low as 0.74%), since it has fewer variations and mutations. Fig. 6

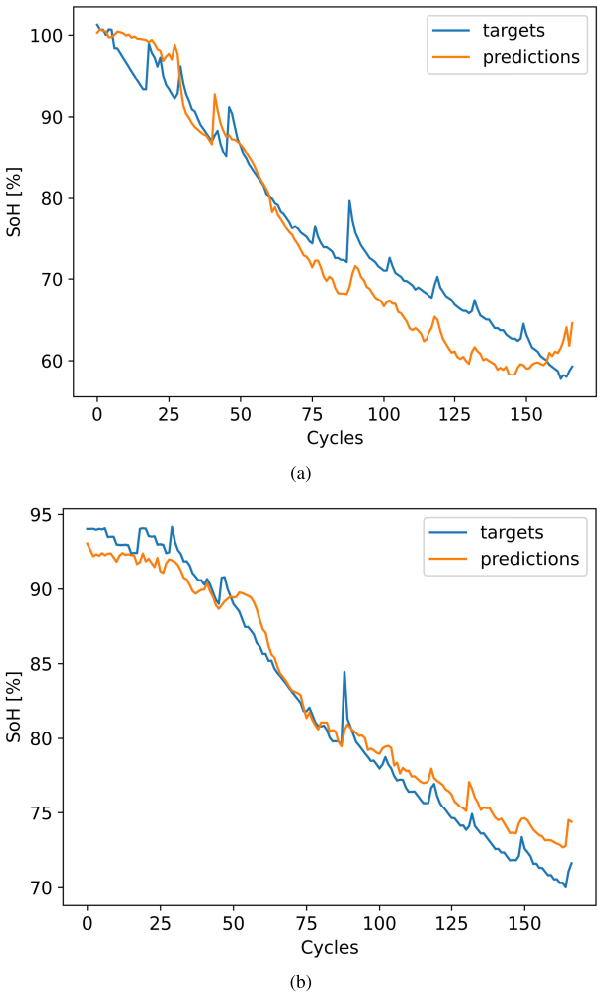

FIGURE 4. SOH ground truths against predictions for the most accurate models in Test Case 3 [Seq. Len. = 1]: (a) B0006: Reformer, (b) B0007: Reformer.

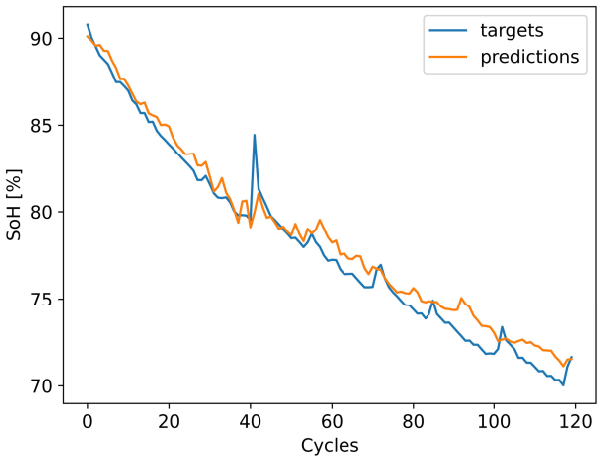

FIGURE 5. SOH ground truths against predictions for the iReformer with B0007 in Test Case 3 [Seq. Len. = 48].

shows how the minimum RMSE achieved with each battery changes with sequence length.

It is obvious as well that the Reformer model, followed by the Transformer, gave the best results in most of the cases whether using regular or inverted embedding. Fig. 7 compares

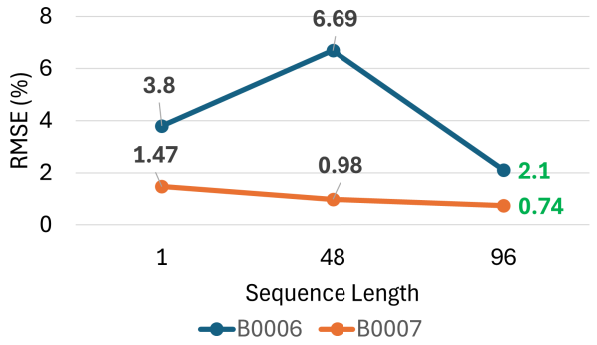

FIGURE 6. The change of the minimum RMSE for each battery changes with sequence length.

the performance of the six models with B0007 (since it showed the best results) at sequence lengths 48 and 96.

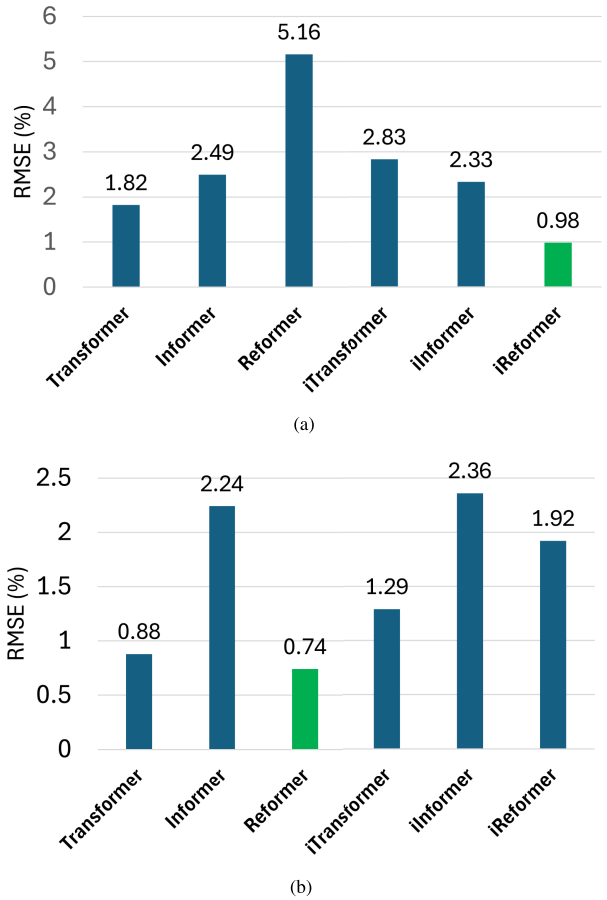

FIGURE 7. RMSE for the six models with B0007: a) Sequence Length = 48, b) Sequence Length = 96.

4) RESULTS COMPARISON

The Reformer model's performance at a sequence length of 48 is compared with six DL models from [41]. The comparison is based on the RMSE achieved for the data in B0007, and is presented in Table 1. The Reformer model demonstrates the lowest RMSE for the same test data (B0007) although being trained solely on the data from B0005, whereas the other models are trained on data from 9 batteries as per the reference manuscript.

TABLE 1. Comparison between the Reformer model (Seq. Len. = 48) and six DL models from [41] using the RMSE for B0007.

Model	RMSE [%]
Reformer	0.98
CNN-BiGRU	1.42
Dilated CNN-BiGRU	1.43
BiGRU	1.94
Dilated CNN	2.07
Dilated CNN-GRU	2.16
Dilated CNN-BiLSTM	2.37

III. STATE OF CHARGE ESTIMATION

A. MODEL ARCHITECTURES

For the estimation of the SOC, we tested the regular and inverted embedding with the three previous models: Transformer, Reformer, and Informer. However, the results were unsatisfactory, and some models failed to converge. A different architecture is used for this problem that is inspired by the study in [35].

In Fig. 8, the SOC estimation architecture is based on a 2-Encoder Transformer model. The first encoder handles the voltage-temperature [V-T] sequence embedding, while the second encoder handles the current-temperature [I-T] one. The extracted contexts from both encoders are concatenated and then passed to the decoder to produce the estimated SOC output. The model is trained on the training segment in the utilized dataset as it comprises a mixture of various charging, discharging, and drive cycle profiles that enable the model to generalize even with unseen testing data. Preliminary results show a high capability for accurately tracking the SOC trends at different experiments, however, the output has significant noise and fluctuations around the true profile. A smoothing strategy is proposed in this study to filter the output by applying a 1D-CNN. A comparison of results is presented in the following test cases to reveal the smoothing effect in different scenarios. Table 2 tabulates the hyperparameters used in the proposed model.

B. DATASET

The experiments were conducted using the *LG 18650HG2* LIB dataset [44]. The dataset was collected at the McMaster Automotive Resource Centre (MARC). It includes a series of tests performed at different temperatures: 25°C, 10°C, 0°C, and -10°C. The dataset contains multiple measurements: time, voltage, current, capacity, energy, power, and battery case temperature. However, during training, validation, and testing, the models use voltage, current, and temperature measurements as input features to estimate the SOC.

This dataset is categorized into training, validation, and testing sets, facilitating model testing and comparison with benchmarks. Additionally, the data includes real-world

TABLE 2. Hyperparameters for SOC estimation model.

Parameter	Value
Encoder layers	4
Decoder layers	4
Attention Heads	1
Dropout	0.14715
Learning Rate	0.00054
Embedding Size	64
1D-CNN Kernel Size	7
Sequence Length	64
Batch Size	128
Number of trainable parameters	2,443,784

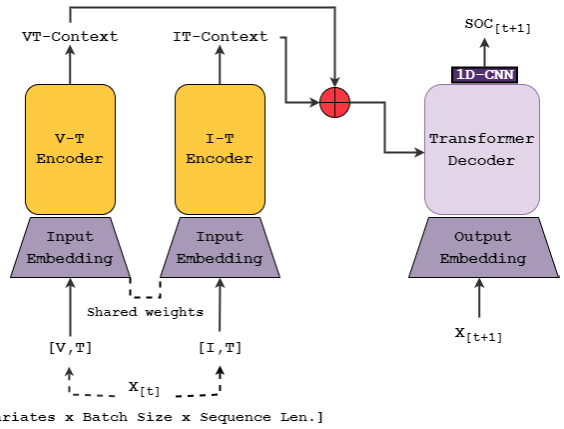

FIGURE 8. 2-Encoder Transformer -> 1D-CNN Architecture for SOC Estimation.

driving cycles such as the Urban Dynamometer Driving Schedule (UDDS), the Highway Fuel Economy Test (HWFET), US06, and LA92 cycles. A mixture of those cycles is used to train the model on [V, I, T] profiles that match those measured in an EV, whether for in-city, highway, or aggressive driving scenarios. A min/max normalization is performed on the data before training and testing as in Eq. 4.

$$x_{normalized} = \frac{x - x_{min}}{x_{max} - x_{min}} \tag{4}$$

Such that x is (V, I, or T) and the x_{min} and x_{max} are the absolute minimum and maximum values for each parameter through the entire dataset. The size of the dataset is tabulated in Table 3.

TABLE 3. The size of the dataset utilized for SOC estimation.

	Training (25%)	Validation (5%)	Testing (20%) -10°C	0°C	10°C	25°C
Data points	669,958	39,295	39,293	42,530	44,284	47,517
Total			882,877			

C. TEST CASES AND RESULTS

1) TEST DATA FROM THE LG DATASET

The first case tests the model with the testing data that are available with the dataset, this data is not experienced by the model during training. The testing data is obtained by concatenating different charging and drive cycle profiles at -10, 0, 10, and 25°C. Fig. 9 shows the smoothing effect of the 1D-CNN at -10°C as an example. The RMSE and the mean absolute error (MAE) for all temperatures are plotted as well before and after smoothing in Fig. 10. A minimum RMSE of 0.91% is achieved by using the 1D-CNN at 25°C.

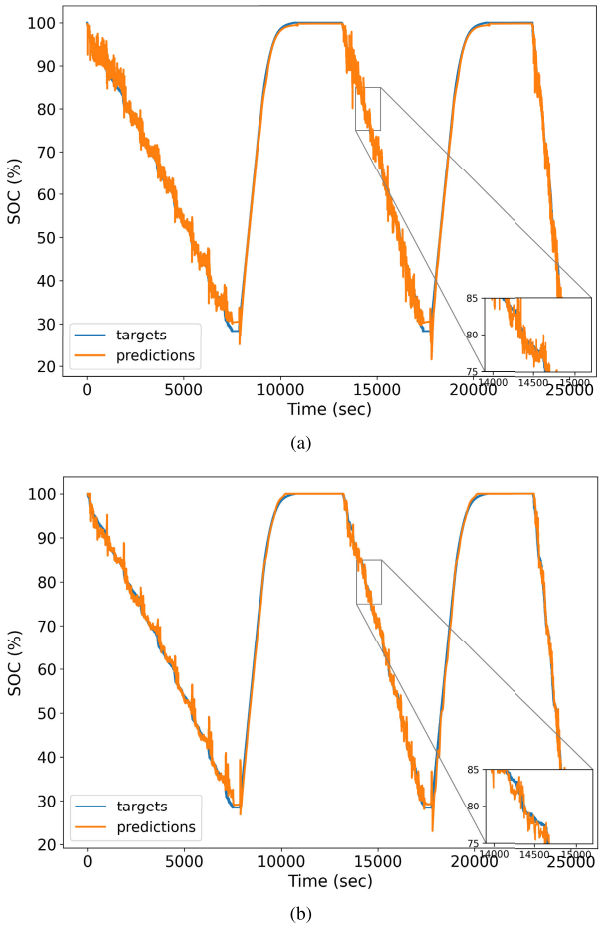

FIGURE 9. Smoothing effect for Test data at -10°C: a) 2-Encoder Transformer, b) 2-Encoder Transformer + 1D-CNN.

2) DRIVE CYCLES

The second test presents the behavior of the proposed model on the UDDS drive cycle at 25°C. Fitting curve is shown in Fig. 11. The RMSE and MAE achieved are 0.93% and 0.74%.

3) ROBUSTNESS TEST (CURRENT OFFSETS)

Here the robustness of the model is tested when there is an offset in the measurements of the current sensor. Four offset values (+/− 0.1A and +/− 0.3A) are added to the current intensity data of the LA92 dataset at -10 °C. Even with a relatively large offset value of +/− 0.3A, the model is robust enough to generalize and produce acceptable estimates,

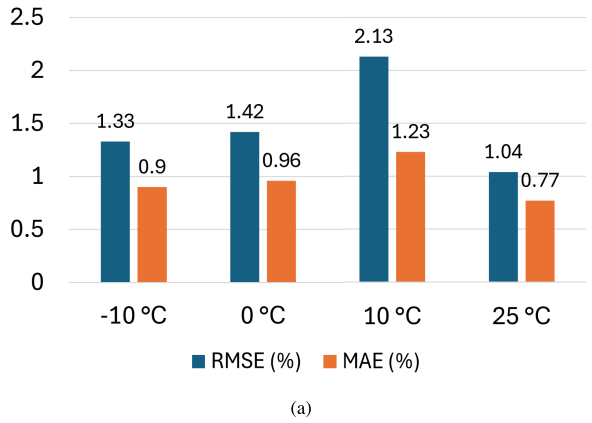

(a)

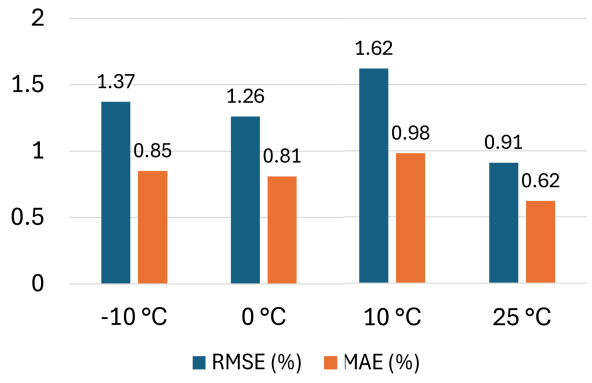

(b)

FIGURE 10. RMSE and MAE for Test data at -10°C: a) 2-Encoder Transformer, b) 2-Encoder Transformer + 1D-CNN.

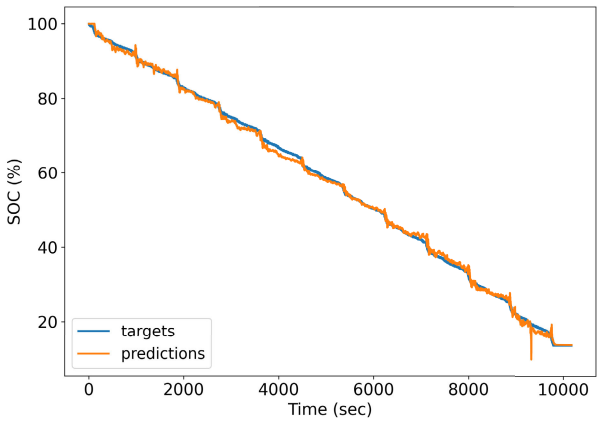

FIGURE 11. 2-Encoder with 1D-CNN for UDDS at 25°C.

which are furtherly smoothed to keep the RMSE below the 2.5%. Fig. 12 shows fitness curve at 0.3A offset together with RMSE and MAE values achieved for all offsets.

4) RESULTS COMPARISON

In order to assess the performance of the proposed model, we compare its accuracy in estimating test data at 25°C to the performance of the DL models described in [40]. The study conducted by Hannan et al. used the raw version of the same dataset. The comparison shown in Table 4 indicates

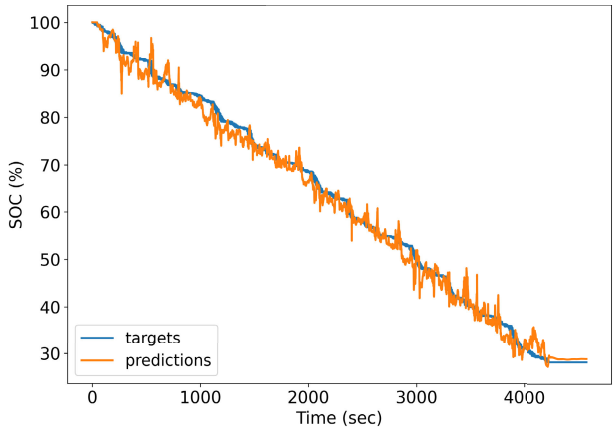

(a)

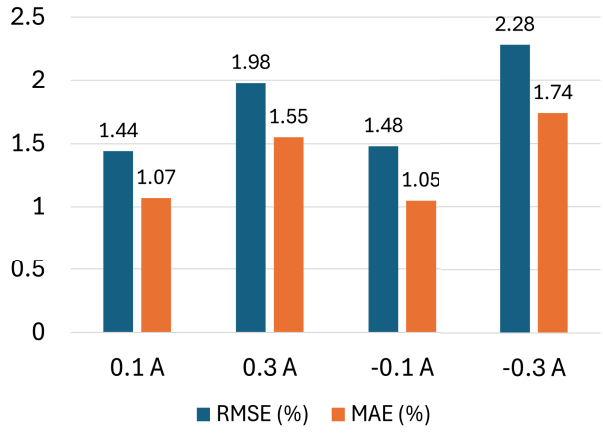

(b)

FIGURE 12. a) LA92 at -10°C with 0.3A offset, b) RMSE and MAE for all current offsets.

that the 2-Encoder Transformer with 1D-CNN architecture produces nearly the same RMSE for SOC percentage as the Transformer model that utilizes self-supervised learning (SSL) at room temperature. The Transformer with SSL is based on a sliding window of the previous 400 steps which adds to the complexity of the architecture, whereas the proposed model relies only on a sequence length of 64 steps.

IV. STATE OF POWER

State of power is defined as how much power a battery can provide for a given period of time without exceeding any operational limits, such as voltage, current, or temperature. In this section, a simple approach to calculating state of power is shown, and the estimated SOC from the prior section is used as an input to the calculation. The approach taken for the calculation of the SOP is not a data-driven one. This is due to the lack of availability of datasets for EVs' SOP. For this reason, the SOP is calculated based on the work in [20]. The maximum amount of power for each charging and discharging case is calculated as in Eq. 5 and 6:

$$P_{max}^{cha} = I_{max}^{cha}(V_{ocv} + I_{max}^{cha}R_{in}) \quad (5)$$

$$P_{max}^{dch} = I_{max}^{dch}(V_{ocv} - I_{max}^{dch}R_{in}) \quad (6)$$

TABLE 4. Comparison between the 2-Encoder 1D-CNN and multiple DL models from [40] using the RMSE for the test data at 25°C.

Model	RMSE [%]
2-Enc. Transformer->1D-CNN (proposed)	0.91
Transformer with SSL	0.91
GRU	1.07
LSTM	1.14
Resnet	1.33
ResCNN	1.35
InceptionTime	1.44
GRU-FCN	1.45
FCN	1.56
LSTM-FCN	1.78
Baseline Transformer	3.60
Deep NN	10.13

I_{max} is the maximum available current in the battery. It has a value for each of charging and discharging. These values are determined from Eq. 7 - 8 as the minimum of the current threshold and the maximum available current with respect to the terminal voltage limit of the battery, as follows:

$$I_{max}^{cha} = min(I_{max,vol}^{cha}, I_{max,cur}^{cha}) \quad (7)$$

$$I_{max}^{dch} = min(I_{max,vol}^{dch}, I_{max,cur}^{dch}) \quad (8)$$

The maximum available current can be calculated from the battery's terminal voltage limit as in Eq. 9 and 10:

$$I_{max,vol}^{cha} = \frac{V_{max} - V_{ocv}}{R_{in}} \quad (9)$$

$$I_{max,vol}^{dch} = \frac{V_{ocv} - V_{min}}{R_{in}} \quad (10)$$

V_{ocv} is determined using the estimated SOC through the battery's SOC-OCV relationship. A polynomial fitting was done for the mapping between the values in the dataset to get a continuous curve to sample from. As can be found in Fig. 13, a polynomial of the tenth degree was the best to describe the relation.

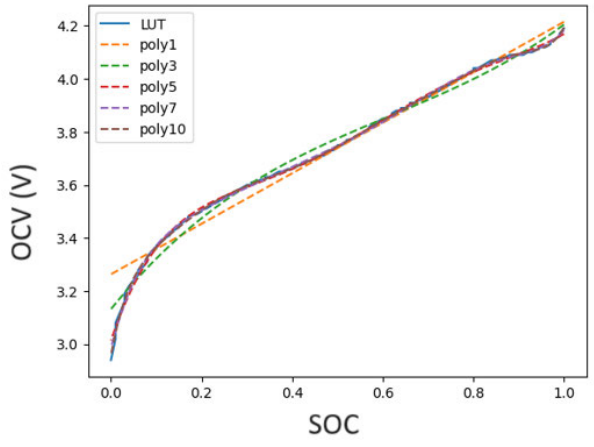

FIGURE 13. Polynomial fitting with different degrees for LG battery's SOC-OCV curve.

R_{in}, V_{max}, and V_{min} were extracted from the specifications for the *LG 18650HG2* LIB as listed in the battery's technical information. A list of the used data can be found in Table 5.

TABLE 5. LG battery information used for calculating the SOP.

Information	Value
R_{in}	0.025Ω
V_{max}	4.2V
V_{min}	2V
$I_{max,cur}^{cha}$	4A
$I_{max,cur}^{dch}$	20A

From the estimated SOC, the SOP can be obtained using the previous equations. Fig. 14 shows a plot of the calculated maximum power that can be supplied by the LG battery based on the SOC estimations done by the 2-Encoder Transformer-CNN model at 25°C for the UDDS cycle. A more precise SOC estimation leads to a more accurate SOP calculation.

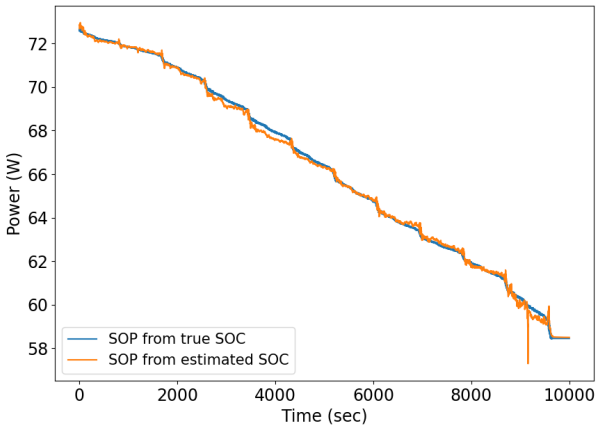

FIGURE 14. The remaining power based on true and estimated SOC for UDDS at 25°C.

V. CONCLUSION AND FUTURE WORK

In this manuscript, a thorough study was conducted to evaluate the effectiveness of different Transformer-based DL models in predicting SOH, SOC, and SOP for LIBs using both regular and inverted embedding techniques. Two real-world datasets were utilized for training, validating, and testing the models for estimating SOC and SOH, while the SOP was derived based on the estimated SOC. For the estimation of SOH, various test cases were conducted using three models: Transformer, Informer, and Reformer, together with their inverted versions. The effect of varying the sequence length is also studied. Aggregation of partial discharge cycles to extract a single feature point of voltage and temperature has been shown to produce the best results, achieving a minimum RMSE of 0.74% using the Reformer model with a sequence length of 96. The regular and inverted architectures of the three previous models did not yield

satisfactory results for SOC estimation. Therefore, a new architecture has been proposed, which is based on a 2-Encoder Transformer followed by a 1D-CNN for smoothing. The model is tested using the test data provided with the dataset to demonstrate the smoothing achieved by the 1D-CNN. An RMSE of 0.91% is obtained for the UDDS drive cycle at 25°C. The model's robustness is also tested by applying offset values to the current intensity measurements. These offsets are up to +/− 0.3A, yet the estimator is still able to generalize. A comparison is conducted for the achieved results with various DL architectures for both SOC and SOH, this shows superiority of the applied Transformer models. The enhanced performance reveals the capability of the context extraction strategy from a sequence which distinguishes the Transformer-based architectures. Finally, the SOP is obtained using calculations from the literature based on the estimated SOC. The deployment of Transformer-based models in real-time on a BMS is a future research interest.

REFERENCES

[1] R. Swarnkar, H. Ramachandran, S. H. M. Ali, and R. Jabbar, "A systematic literature review of state of health and state of charge estimation methods for batteries used in electric vehicle applications," *World Electr. Vehicle J.*, vol. 14, no. 9, p. 247, Sep. 2023.

[2] V. Masson-Delmotte, P. Zhai, H.-O. Pörtner, D. Roberts, J. Skea, and P. R. Shukla, *Global Warming of 1.5°C: IPCC Special Report on Impacts of Global Warming of 1.5°C Above Pre-Industrial Levels in Context of Strengthening Response to Climate Change, Sustainable Development, and Efforts to Eradicate Poverty*. Cambridge, U.K.: Cambridge Univ. Press, 2022.

[3] T. Watari, B. McLellan, S. Ogata, and T. Tezuka, "Analysis of potential for critical metal resource constraints in the international energy agency's long-term low-carbon energy scenarios," *Minerals*, vol. 8, no. 4, p. 156, Apr. 2018.

[4] S. S. Kamran, A. Haleem, S. Bahl, M. Javaid, C. Prakash, and D. Budhhi, "Artificial intelligence and advanced materials in automotive industry: Potential applications and perspectives," *Mater. Today, Proc.*, vol. 62, pp. 4207–4214, 2022. https://www.sciencedirect.com/science/article/pii/S2214785322028954

[5] S. Katreddi, S. Kasani, and A. Thiruvengadam, "A review of applications of artificial intelligence in heavy duty trucks," *Energies*, vol. 15, no. 20, p. 7457, Oct. 2022. [Online]. Available: https://www.mdpi.com/1996-1073/15/20/7457

[6] T. G. Canada. (2050). *Net-Zero Emissions by 2050*. [Online]. Available: https://www.canada.ca/en/services/environment/weather/climatechange/climate-plan/net-zero-emissions-2050.html

[7] T. Canada. (Jun. 2021). *Building a Green Economy: Government of Canada to Require 100% of Car and Passenger Truck Sales be Zero-Emission by 2035 in Canada*. [Online]. Available: https://www.canada.ca/en/transport-canada/news/2021/06/building-a-green-economy-government-of-canada-to-require-100-of-car-and-passenger-truck-sales-be-zero-emission-by-2035-in-canada.html

[8] K. S. Ng, C.-S. Moo, Y.-P. Chen, and Y.-C. Hsieh, "Enhanced Coulomb counting method for estimating state-of-charge and state-of-health of lithium-ion batteries," *Appl. Energy*, vol. 86, no. 9, pp. 1506–1511, Sep. 2009.

[9] J. Yan, G. Xu, H. Qian, and Y. Xu, "Robust state of charge estimation for hybrid electric vehicles: Framework and algorithms," *Energies*, vol. 3, no. 10, pp. 1654–1672, Sep. 2010.

[10] W. He, N. Williard, C. Chen, and M. Pecht, "State of charge estimation for electric vehicle batteries using unscented Kalman filtering," *Microelectron. Rel.*, vol. 53, no. 6, pp. 840–847, Jun. 2013.

[11] J. Belt, V. Utgikar, and I. Bloom, "Calendar and PHEV cycle life aging of high-energy, lithium-ion cells containing blended spinel and layered-oxide cathodes," *J. Power Sources*, vol. 196, no. 23, pp. 10213–10221, Dec. 2011.

[12] L. Lombardi, B. Ospina Agudelo, W. Zamboni, and E. Monmasson, "Battery aging models based on high-current incremental capacity in fast charging," *Batteries*, vol. 9, no. 1, p. 2, Dec. 2022.

[13] Y. Li, K. Liu, A. M. Foley, A. Zülke, M. Berecibar, E. Nanini-Maury, J. Van Mierlo, and H. E. Hoster, "Data-driven health estimation and lifetime prediction of lithium-ion batteries: A review," *Renew. Sustain. Energy Rev.*, vol. 113, Oct. 2019, Art. no. 109254.

[14] S. Park, J. Ahn, T. Kang, S. Park, Y. Kim, I. Cho, and J. Kim, "Review of state-of-the-art battery state estimation technologies for battery management systems of stationary energy storage systems," *J. Power Electron.*, vol. 20, no. 6, pp. 1526–1540, Nov. 2020.

[15] J. Lu, Z. Chen, Y. Yang, and L. V. Ming, "Online estimation of state of power for lithium-ion batteries in electric vehicles using genetic algorithm," *IEEE Access*, vol. 6, pp. 20868–20880, 2018.

[16] C. Hu, B. D. Youn, and J. Chung, "A multiscale framework with extended Kalman filter for lithium-ion battery SOC and capacity estimation," *Appl. Energy*, vol. 92, pp. 694–704, Apr. 2012.

[17] G. L. Plett, "Extended Kalman filtering for battery management systems of LiPB-based HEV battery packs," *J. Power Sources*, vol. 134, no. 2, pp. 252–261, Aug. 2004.

[18] G. L. Plett, "Extended Kalman filtering for battery management systems of LiPB-based HEV battery packs: Part 3. State and parameter estimation," *J Power Sources*, vol. 134, pp. 277–292, Aug. 2004.

[19] S. Rahimifard, S. Habibi, and J. Tjong, "Dual estimation strategy for new and aged electric vehicles batteries," in *Proc. IEEE Transp. Electrific. Conf. Expo (ITEC)*, Jun. 2020, pp. 579–583.

[20] S. Rahimifard, S. Habibi, G. Goward, and J. Tjong, "Adaptive smooth variable structure filter strategy for state estimation of electric vehicle batteries," *Energies*, vol. 14, no. 24, p. 8560, Dec. 2021.

[21] L. Wang, J. Ma, X. Zhao, X. Li, and K. Zhang, "Online estimation of state-of-charge inconsistency for lithium-ion battery based on SVSF-VBL," *J. Energy Storage*, vol. 67, Sep. 2023, Art. no. 107657.

[22] C. Chen, B. Zhang, G. Vachtsevanos, and M. Orchard, "Machine condition prediction based on adaptive neuro–fuzzy and high-order particle filtering," *IEEE Trans. Ind. Electron.*, vol. 58, no. 9, pp. 4353–4364, Sep. 2011.

[23] M. Zhang, Y. Liu, D. Li, X. Cui, L. Wang, L. Li, and K. Wang, "Electrochemical impedance spectroscopy: A new chapter in the fast and accurate estimation of the state of health for lithium-ion batteries," *Energies*, vol. 16, no. 4, p. 1599, Feb. 2023. [Online]. Available: https://www.mdpi.com/1996-1073/16/4/1599

[24] M.-K. Tran, M. Mathew, S. Janhunen, S. Panchal, K. Raahemifar, R. Fraser, and M. Fowler, "A comprehensive equivalent circuit model for lithium-ion batteries, incorporating the effects of state of health, state of charge, and temperature on model parameters," *J. Energy Storage*, vol. 43, Nov. 2021, Art. no. 103252.

[25] M. Ismail, R. Dlyma, A. Elrakaybi, R. Ahmed, and S. Habibi, "Battery state of charge estimation using an artificial neural network," in *Proc. IEEE Transp. Electrific. Conf. Expo (ITEC)*, Jun. 2017, pp. 342–349.

[26] (2023). *Stanford University Human-Centered Artificial Intelligence*. [Online]. Available: https://aiindex.stanford.edu/report/

[27] D. M. Ahmed, M. M. Hassan, and R. J. Mstafa, "A review on deep sequential models for forecasting time series data," *Appl. Comput. Intell. Soft Comput.*, vol. 2022, pp. 1–19, Jun. 2022.

[28] Y. Li, M. Du, and S. He, "Attention-based sequence-to-sequence model for time series imputation," *Entropy*, vol. 24, no. 12, p. 1798, Dec. 2022. [Online]. Available: https://www.mdpi.com/1099-4300/24/12/179

[29] H. Abbasimehr and R. Paki, "Improving time series forecasting using LSTM and attention models," *J. Ambient Intell. Humanized Comput.*, vol. 13, no. 1, pp. 673–691, Jan. 2022.

[30] M. Wand, J. Koutník, and J. Schmidhuber, "Lipreading with long short-term memory," in *Proc. IEEE Int. Conf. Acoust., Speech Signal Process. (ICASSP)*, Mar. 2016, pp. 6115–6119.

[31] E. Chemali, P. J. Kollmeyer, M. Preindl, R. Ahmed, and A. Emadi, "Long short-term memory networks for accurate state-of-charge estimation of Li-ion batteries," *IEEE Trans. Ind. Electron.*, vol. 65, no. 8, pp. 6730–6739, Aug. 2018.

[32] M. Schuster and K. K. Paliwal, "Bidirectional recurrent neural networks," *IEEE Trans. Signal Process.*, vol. 45, no. 11, pp. 2673–2681, 1997.

[33] A. Vaswani, N. Shazeer, N. Parmar, J. Uszkoreit, L. Jones, A. N. Gomez, Ł. Kaiser, and I. Polosukhin, "Attention is all you need," in *Proc. Adv. Neural Inf. Process. Syst.*, vol. 30, 2017, pp. 1–11.

[34] N. Sitapure and A. Kulkarni, "Exploring different time-series-transformer (TST) architectures: A case study in battery life prediction for electric vehicles (EVs)," 2023, *arXiv:2308.03260*.
[35] H. Shen, X. Zhou, Z. Wang, and J. Wang, "State of charge estimation for lithium-ion battery using transformer with immersion and invariance adaptive observer," *J. Energy Storage*, vol. 45, Jan. 2022, Art. no. 103768.
[36] Z. Yi, L. Wang, and K. Yang, "State of charge estimation for lithium-ion battery using time series transformer with de-noise de-stationary inception network," *J. Energy Storage*, vol. 93, Jul. 2024, Art. no. 112224.
[37] H. Zhou, S. Zhang, J. Peng, S. Zhang, J. Li, H. Xiong, and W. Zhang, "Informer: Beyond efficient transformer for long sequence time-series forecasting," in *Proc. AAAI Conf. Artif. Intell.*, May 2021, vol. 35, no. 12, pp. 11106–11115.
[38] N. Kitaev, Ł. Kaiser, and A. Levskaya, "Reformer: The efficient transformer," 2020, *arXiv:2001.04451*.
[39] Y. Liu, T. Hu, H. Zhang, H. Wu, S. Wang, L. Ma, and M. Long, "ITransformer: Inverted transformers are effective for time series forecasting," 2023, *arXiv:2310.06625*.
[40] M. A. Hannan, D. N. T. How, M. S. H. Lipu, M. Mansor, P. J. Ker, Z. Y. Dong, K. S. M. Sahari, S. K. Tiong, K. M. Muttaqi, T. M. I. Mahlia, and F. Blaabjerg, "Deep learning approach towards accurate state of charge estimation for lithium-ion batteries using self-supervised transformer model," *Sci. Rep.*, vol. 11, no. 1, p. 19541, Oct. 2021.
[41] Z. Bao, J. Jiang, C. Zhu, and M. Gao, "A new hybrid neural network method for state-of-health estimation of lithium-ion battery," *Energies*, vol. 15, no. 12, p. 4399, Jun. 2022. [Online]. Available: https://www.mdpi.com/1996-1073/15/12/4399
[42] B. Saha and K. Goebel, "Battery data set," NASA AMES Prognostics Data Repository, Moffett Field, CA, USA, Tech. Rep. DASHLINK_133, 2007.
[43] J. Duque, P. J. Kollmeyer, and M. Naguib, "Battery aging dataset for 15 minute fast charging of Samsung 30T cells," McMaster Univ., Hamilton, ON, Canada, Tech. Rep., 2023, doi: 10.17632/cp3473x7xv.3.
[44] P. Kollmeyer, C. Vidal, M. Naguib, and M. Skells, "LG 18650HG2 Li-ion battery data and example deep neural network xEV SOC estimator script," McMaster Univ., Hamilton, ON, Canada, Tech. Rep., 2020, doi: 10.5683/SP3/UYPYDJ.

JOHN GUIRGUIS received the B.Sc. and M.Sc. degrees in mechanical engineering from Ain Shams University, Cairo, Egypt, in 2017 and 2023, respectively. He is currently pursuing the Ph.D. degree in mechanical engineering with McMaster University, Hamilton, ON, Canada.

From 2018 to 2023, he joined the Mechatronics Department, Ain Shams University, as a full-time TA and RA. His research interests include control and management of Li-Ion batteries for EV applications, model-based and data-driven state estimation, tracking control for autonomous vehicles, advanced control theories, artificial intelligence, and machine learning.

AHMED ABDULMAKSOUD received the B.Sc. degree in electrical engineering from Ain Shams University, Cairo, Egypt, in 2023. He is currently pursuing the M.A.Sc. degree in mechanical engineering with McMaster University, Hamilton, ON, Canada.

From 2022 to 2023, he was a Software Engineer Intern with Siemens Digital Industry Software, Cairo. From 2022 to 2023, he was also the Autonomous Perception Lead of the ASU Racing Team's Autotronics Research Laboratory, Cairo, specifically for the formula student AI competition in the U.K. working on autonomous racing cars and autonomous drones for environment mapping. His research interests include machine learning applications in robotics, electrical vehicles, autonomous perception, 3D scanning, and the utilization of cloud and distributed software systems across various engineering domains.

MOHANAD ISMAIL received the B.Sc. degree in electrical engineering from Ain Shams University, Cairo, Egypt, in 2023. He is currently pursuing the M.A.Sc. degree in mechanical engineering with McMaster University, Hamilton, ON, Canada.

From 2022 to 2023, he was a Software Engineer Intern with Dell Technologies, Cairo. His research interests include the application of cloud technologies and distributed software systems in different domains, including mechanical engineering applications, such as electric vehicles and battery management systems.

PHILLIP J. KOLLMEYER (Member, IEEE) received the B.S., M.S., and Ph.D. degrees in electrical engineering from the University of Wisconsin–Madison, in 2006, 2011, and 2015, respectively. In July 2023, he started as an Assistant Professor with McMaster University, where he was a Senior Principal Research Engineer, from 2019 to 2023, and a Postdoctoral Research Associate, from 2016 to 2019. His research interests include the battery area with topics, including state estimation, modeling, aging, ultra-fast charging, thermal management and on optimizing electric drivetrain efficiency via multi-speed gearboxes, wide bandgap power electronics, and power split control algorithms. He has authored or co-authored more than 75 publications, acted in a supervisory role for more than a dozen graduate students, and created several widely utilized open-source battery datasets and algorithms. From 2018 to 2023, he served on the senior organizing committee of the IEEE Transportation Electrification Conference (ITEC) and he was the General Chair of the Conference, in 2023.

RYAN AHMED received the M.B.A. degree in finance from the DeGroote School of Business, the Master of Applied Science (M.A.Sc.) degree from McMaster University, focusing on artificial intelligence and fault detection, and the Ph.D. degree in engineering, focusing on battery modeling, state of charge, and state of health estimation. He is currently an Assistant Professor with the Department of Mechanical Engineering, McMaster University. His research interests include smart systems, artificial intelligence, energy storage devices, autonomous systems, and electric powertrains. Prior to joining McMaster, he held several senior engineering positions globally with General Motors, Stellantis, and Samsung. He taught several courses on science, technology, engineering, and mathematics to over more than 370 000 students from 160 countries with more than 29 000 five-star reviews and an overall rating of 4.5/5. He is the principal author or co-author of over 35 journals and conference publications. He was a co-recipient of two best papers awards at IEEE TRANSACTIONS ON INDUSTRIAL ELECTRONICS, in 2018, and at the IEEE Transportation Electrification Conference and Expo (ITEC 2012), Detroit, MI, USA. He is also a Stanford Certified Project Manager (SCPM) and a Certified Professional Engineer (P.Eng.) in Ontario. He was the Program Co-Chair of the 2017 IEEE Transportation and Electrification Conference (iTEC'17), Chicago, IL, USA.